The use of chitosan as an effective carrier of theophylline – an anti-asthmatic drug

Noor Firas Aziz[1] (ORCID ID: 0000-0002-6479-1089), **Samer Hasan Hussein-Al-Ali**[1), 2), *] (0000-0002-8760-6069), **Mowafaq Mohammed Ghareeb**[3], **Nashwan Abdallah Nashwan**[4] (0000-0001-7257-4394)

DOI: https://doi.org/10.14314/polimery.2023.3.4

Abstract: In order to solve the problem of frequent drug dosing and increase its effectiveness, theophylline (THP) was deposited on chitosan nanoparticles (CSNPs). THP-CSNPs nanocomposites with the composition of 50, 75, 100 or 150 mg of chitosan (CS) and 25, 50, 75, 100 or 200 mg of tripolyphosphate (TPP) at pH 4.0, 5.0, 6.0 and 6.5 were prepared, and a constant weight of THP of 100 mg. The nanocomposites were characterized by X-ray diffraction (PXRD), field emission scanning electron microscopy (FE-SEM), and Fourier transform infrared spectroscopy (FTIR). The rate of drug release was also tested. The Minitab 18 program was used to analyze the results. The independent variables were the CS, TPP, and pH, while loading efficiency, zeta potential, and particle size were the dependent variables. The nanocomposites successfully transported and protected the drug, providing its sustained release.

Keywords: theophylline, chitosan, nanocomposites, controlled drug release.

Zastosowanie chitozanu jako skutecznego nośnika teofiliny – leku przeciwastmatycznego

Streszczenie: W celu rozwiązania problemu częstego dawkowania leku i zwiększenia jego efektywności teofilinę (THP) osadzono na nanocząstkach chitozanu (CSNPs). Przygotowano nanokompozyty THP-CSNPs o składzie 50, 75, 100 lub 150 mg chitozanu (CS) oraz 25, 50, 75, 100 lub 200 mg trójpolifosforanu (TPP) przy pH 4,0, 5,0, 6,0 i 6,5 oraz stałej masie THP wynoszącej 100 mg. Nanokompozyty charakteryzowano za pomocą dyfrakcji promieniowania rentgenowskiego (PXRD), skaningowej mikroskopii elektronowej z emisją polową (FE-SEM), spektroskopii w podczerwieni z transformacją Fouriera (FTIR). Zbadano również szybkość uwalniania leku. Do analizy wyników wykorzystano program Minitab 18. Niezależnymi zmiennymi były CS, TPP i pH, podczas gdy wydajność ładowania, potencjał zeta i wielkość cząstek były zmiennymi zależnymi. Nanokompozyty z powodzeniem transportowały i zabezpieczały lek, zapewniając jego przedłużone uwalnianie.

Słowa kluczowe: teofilina, chitozan, nanokompozyty, kontrolowane uwalnianie leków.

Athletes' success depends on their skills and other abilities. However, many athletes have been found to consume theophylline (THP) to enhance their performance [1]. Still, studies show no ergogenic effects of THP, suggesting that the drug should remain acceptable for athletes with asthma participating in international sporting events [2, 3]. THP has been used to treat respiratory diseases, including exercise-induced bronchospasm [4], for over 90 years. THP decreases exhaustion of certain muscle groups in humans, providing a theoretical basis for a positive effect in sporting activity [5, 6]. The studies also show that therapeutic levels of THP had no impact on fatigability or strength during maximal contraction in any muscle group studies [7]. One study showed THP significantly increased the endurance of forearm musculature by delaying the onset of intracellular metabolic acidosis [8].

Controlled drug delivery has been the primary focus of research in pharmacy [9]. The controlled delivery system exhibits a pattern of drug release in which the drug concentration remains in the therapeutic window for a sufficiently long time, achieving a sustained physiological effect. Polymers have achieved successful applications in the formulation of controlled drug delivery [10]. Their small size provides different benefits, such as sustained residence in gastro intestinal tract (GIT), better penetra-

[1)] Department of Basic Pharmaceutical Sciences, Faculty of Pharmacy, Isra University, Amman 11622, Jordan.

[2)] Department of Chemistry, Faculty of Sciences, Isra University, Amman 11622, Jordan.

[3)] Division of Pharmaceutics, College of Pharmacy, University of Baghdad, Baghdad, 10047, Iraq.

[4)] Faculty of Arts, Isra University, Amman 11622, Jordan.

[*)] Author for correspondence: samer.alali@iu.edu.jo, sameralali72@yahoo.com

tion, and excellent cell uptake [11]. Additionally, these nanoparticles are highly degradable with little toxicity to cells [12]. These properties make them excellent candidates for increasing effectiveness. Nanoparticles have several advantages, such as better in vivo stability, long-term capacity release, and permeation through tiny capillaries and body compartments [13]. Furthermore, nanoparticles could increase the drug's therapeutic index, change pharmacokinetic and biodistribution properties, and assist in sustained-release reservoir formation [14].The main requirements for nanoparticle design include small size (50–200 nm), high loading capacity, slow complex dissociation in vivo, and optimized targeting to the desired tissue with limited absorption by other tissues. Developing a formulation with such characteristics while considering design simplicity and cost is crucial for an effective drug delivery system [15, 16].

Chitosan is an N-deacetylated chitin derivative, a linear polysaccharide formed from randomly arranged deacetylated units of β-(1-4)-linked D-glucosamine along with acetylated units of N-acetyl-D-glucosamine. Chitosan is made by treating chitin harvested from shrimp and other shellfish shells with alkaline sodium hydroxide. [17].

Theophylline (dimethyl xanthine) has been prescribed to manage pulmonary diseases for a long time. The drug acts as a bronchodilator. However, for it to be effective, relatively high doses need to be prescribed, which increases the likelihood of many adverse effects associated with the medication. Frequent side effects have depopularized theophylline administration, increasing preference for inhaled b2-agonists. Recently, it has been proven that in lower concentrations theophylline has an anti-inflammatory effect on asthma and chronic obstructive pulmonary disease (COPD) [4].

Most drugs have drawbacks such as poor stability, water insolubility, low selectivity, high toxicity, and adverse effects. Drug carriers should play a vital role in overcoming these obstacles. Nanoparticles of chitosan are drug carriers having the convenience of extended drug release, which controls the solubility and stability of the drug while simultaneously enhancing efficacy and reducing toxicity [18].

The administration of drugs as a single dose rather than multiple doses has been made available using sustained-release preparations. Prolonging the release of the drug enables a constant level of the drug in the blood.

Theophylline (THP) is administered orally, intravenously, or inhaled as an anti-asthma treatment [19, 20]. Although, recent research revealed that the dose range of THP, which is optimized between efficacy and toxicity, is narrow (the therapeutic index of THP is between 10 to 20 μg/mL) [21]. In addition, the short half-life of THP may cause poor patient compliance due to the frequent administration of the medicine. Therefore, we used the THP drug as a model to form THP-CS nanocomposites.

In this study, the design of experiments included many interrelated activities; for example, the development of statistical hypotheses correlated closely with the scientific hypothesis and the selection of the independent variables to be controlled and dependent variables. Additionally, we classified the randomization procedure to choose the experimental units. Nevertheless, the design of the experiments included the statistical analysis used to illustrate the correlation between independent and dependent variables.

The present work aims to optimize theophylline-loaded chitosan nanoparticles and analyze different variables (tripolyphosphate, chitosan concentration, and pH value) on the loading efficiency, zeta potential, and particle size of nanocomposites.

EXPERIMENTAL PART

Materials

All chemicals, reagents, solvents, and metal salts used were of analytical grade. Theophylline (99%), sodium tripolyphosphate (TPP), and chitosan with low molecular weight (10–120kD$_a$) were purchased from Sigma Aldrich (USA). Acetic acid and sodium hydroxide were purchased from Chem Co (England).

Preparation of CSNPs nanoparticles

Chitosan nanoparticles were prepared by dissolving 500 mg of chitosan in 10 ml of acetic acid heated to 45°C, stirring the sample until a uniform solution was achieved. The 500 ml volumetric flask was topped off with distilled water. 100 ml of this solution was transferred to a new 500 ml volumetric flask, and tripolyphosphate was titrated dropwise to form chitosan nanoparticles (CSNPs). Many researchers employed tripolyphosphate for chitosan nanoparticles preparation due to its favorable characteristics, such as nontoxicity, multivalence, and capability of making gels via ionic gelation due to its negative charge.

Preparation of THP-CSNPs nanocomposites

Theophylline-chitosan nanocomposites were prepared according to previously published research with some modifications [22]. Briefly, various quantities of chitosan were dissolved in acetic acid under hot magnetic stirring (45°C). As the chitosan amount increased, so did the amount of acetic acid needed to dissolve chitosan. Tripolyphosphate was added to the chitosan-acetic acid solution dropwise to form CSNPs. Next, 100 mg of theophylline was liquefied in 15 ml of sodium hydroxide and topped off to 25 ml using deionized water. This solution was then added to chitosan nanoparticles to form THP-CSNPs. pH was monitored and adjusted as needed, using NaOH to achieve the specified pH (4.0, 5.0, 6.0, and 6.5). THP-CSNP mixture was stirred for 18 h and then centrifuged for 10–45 min, depending on the amount of

chitosan added to the sample, at 11,000 rpm. After completing the centrifugation, a gel and a supernatant were obtained. The gel was dried in an oven at 40°C for two days to get a dry powder of THP-CSNPs.

In vitro release study

The release of theophylline was examined in PBS at pH 7.4 and λ_{max} of 271 nm. A sufficient weight of each nanocomposite was added to the release media. The cumulative dissolved concentration of theophylline was measured using a calibration curve.

The percent release of theophylline in the PBS was calculated from Equation 1.

$$\%\text{Release} = \frac{\text{Mass of THP at time } t}{\text{Mass of THP in nanocomposite}} \cdot 100 \quad (1)$$

Determination of loading efficiency (%LE)

The supernatant from the centrifugation step used to prepare THP-CSNP was used to measure the loading efficiency (LE) of theophylline from prepared nanocomposites. The sample was centrifuged (Hettich Universal 30 RF, Germany) at 11,000 rpm for 45 minutes. The supernatant was separated from the gel. The free drug in the supernatant was measured from the absorbance at λ_{max} of 271 nm by UV-vis spectrophotometer, and the loading efficiency of theophylline was calculated from Equation 2.

$$\%\text{Loading} = \frac{\text{Total mass of THP} - \text{Total mass of free THP}}{\text{Mass of nanocomposites}} \cdot 100 \quad (2)$$

Full factorial design (FFD) for design of experiments

In the current study, the effect of CS, TPP, and pH, the three independent variables, on the loading efficiency, zeta potential, and particle size, three dependent variables, were investigated using Minitab 18 software. According to the applied design, 80 experimental runs were performed in random order. Graphical analyses, such as contour, surface, main effects, and interaction plots, were performed. Degree of freedom (DF), an adjusted sum of square (Adj SS), adjusted mean square (Adj MS), coefficient (Coef), square error of coefficient (SE Coef), F-value, T-value, P-value, and VIF were used in the analysis. Table 1 shows all collected data.

T a b l e 1. Levels of CS, TPP and pH

Parameter	Levels				
	1	2	3	4	5
Chitosan, mg	50	75	100	150	–
TPP, mg	25	50	75	100	200
pH	4	5	6	6.5	–

Ultraviolet spectrophotometry

Ultraviolet-visible spectrophotometry is a widespread technique used to qualitatively and quantitatively characterize samples. The absorbance was measured at λ_{max}=271 nm to identify the concentration of free drug (THP) in the supernatant of the sample solution after centrifugation. These measurements allow for determining the percentage of efficiency in the theophylline-loaded nanocomposites. Additionally, *in vitro* release of THP can be determined in PBS (pH=7.4) by the same technique.

Fourier transform infrared spectroscopy (FTIR)

FTIR is used to identify functional groups and chemical bonds in a molecule from the infrared absorption spectrum. Because each functional group has its unique wavelength and absorption properties, the functional groups in a sample can be identified, and the structure of the entire molecule deduced. Thus, this technique can support data on molecular interaction and compatibility recorded using other experimental approaches. The spectra were obtained in the range of 400–4000 cm^{-1} on a Perkin Elmer with 4 cm^{-1} resolutions. A small amount of powder sample was used (0.01mg), and the force applied to the powder was about 75 N. The instrument and die were cleaned with ethanol after the analysis.

Particle size and zeta potential of THP-CSNPs nanocomposites

THP-CSNP particle size was measured using dynamic light scattering (DLS) with Zetasizer (Malvern, UK) at Hikma Pharmaceutical Manufacturing. Each sample was analyzed in triplicate at 25°C. The samples were dispersed in distilled water and sonicated for 15 minutes. The cuvette was filled and capped. The Malvern logo faced the instrument front. There were no bubbles in the cuvette. The software automatically recorded run numbers for each measurement.

Powder X-ray diffraction (PXRD)

The PXRD is a technique used to give information on the unit cell dimensions and phase identification of crystalline material. The PXRD technique was used in the range of 5–70° with an XRD D5005 diffractometer with Cu radiation (Siemens, Munich, Germany).

Field emission scanning electron microscopy (FE-SEM)

Field emission scanning electron microscopy (FE-SEM) is a technique used to capture microstructure images of materials. A Zeiss LEO 1550 (Jena, Germany) scanning electron microscope (FE-SEM) was used for the analysis.

T a b l e 2. Results data for LE, zeta potential, and particle size for nanocomposites

Sample code	CS	TPP	pH	%LE	Particle Size	Zeta Potential	Sample code	CS	TPP	pH	%LE	Particle Size	Zeta Potential	Sample code	CS	TPP	pH	%LE	Particle Size	Zeta Potential
1	75	25	6	78	–	0.81	28	150	25	6.5	91	296	-4.24	55	100	200	5	–	368	-7.62
2	100	100	6	59	250	1.51	29	50	50	6	75	348	2.33	56	100	75	4	50	309	-0.83
3	100	200	6	50	290	–	30	100	75	4	–	242	1.75	57	100	25	4	88	162	–
4	75	75	6.5	63	442	–	31	50	25	6.5	88	409	-1.08	58	150	200	6.5	59	187	-0.95
5	100	25	5	–	250	2.92	32	50	50	5	70	180	7.44	59	150	75	6	62	–	-1.13
6	75	100	6	69	198	-7.37	33	150	50	4	86	312	1.85	60	100	25	6.5	70	–	5.48
7	50	75	4	–	250	1.53	34	150	25	6	92	225	-1.06	61	150	75	4	–	331	–
8	50	75	6.5	–	300	-1.33	35	75	75	4	73	292	–	62	150	200	5	63	314	-4.44
9	150	50	5	71	124	–	36	50	200	6	68	–	–	63	100	50	5	67	119	–
10	50	100	5	75	196	-7.39	37	150	25	4	90	250	–	64	75	25	4	91	110	7.08
11	75	50	6.5	68	250	3.54	38	75	50	4	70	203	13.07	65	150	50	6.5	86	268	-7.62
12	150	100	5	–	–	–	39	100	50	6.5	–	–	-3.44	66	150	100	4	80	276	v
13	100	50	6	–	–	-3.73	40	150	50	6	84	250	-3.63	67	75	75	5	60	146	10.02
14	100	75	6.5	53	–	-1.02	41	75	200	5	64	357	2.51	68	75	75	6	66	379	–
15	50	50	6.5	78	290	-6.83	42	75	50	5	–	162	6.82	69	50	25	5	–	119	3.57
16	100	100	4	54	204	2.58	43	100	75	5	53	232	6.83	70	50	100	6	–	306	–
17	75	50	6	–	338	-3.83	44	150	100	5	59	–	2.51	71	50	25	4	90	104	20.61
18	75	100	5	63	–	-1.81	45	150	100	6.5	62	329	-2.06	72	75	100	6.5	74	425	–
19	75	25	6.5	91	341	–	46	100	200	4	–	391	-0.26	73	100	75	6	51	152	–
20	50	100	6.5	85	376	-4.44	47	100	100	6.5	57	208	-0.08	74	50	200	6.5	72	250	–
21	50	200	4	77	–	-0.34	48	150	75	6.5	66	250	-4.09	75	50	25	6	–	173	2.52
22	100	25	6	–	309	–	49	150	25	5	81	84	1.25	76	75	200	6.5	72	–	-9.12
23	50	50	4	79	–	13.91	50	100	50	4	85	163	15.30	77	50	75	5	83	–	1.17
24	75	25	5	–	146	11.11	51	50	75	5	70	250	2.52	78	50	100	4	83	250	1.53
25	75	100	4	71	–	-2.01	52	150	200	6	55	258	-2.12	79	50	75	6	–	284	-11.37
26	150	75	5	83	250	-0.12	53	150	100	6	75	250	-0.42	80	50	200	5	83	383	-10.26
27	100	100	5	66	298	0.62	54	75	200	6	73	270	–							

T a b l e 3. ANOVA data for %LE, particle size, and zeta potential

LE model						Particle size model						Zeta potential model					
Source	Adj SS	Adj MS	F Value	P Value	VIF	Source	Adj SS	Adj MS	F Value	P Value	VIF	Source	Adj SS	Adj MS	F Value	P Value	VIF
Model	5966.87	662.99	12.88	0.000	–	Model	261482	29053.6	8.21	0.000	–	Model	1409.85	156.650	9.17	0.000	–
Linear	2835.46	945.15	18.36	0.000	1.31	Linear	104191	34730.5	9.81	0.000	1.43	Linear	715.68	238.561	13.96	0.000	1.55
CS	289.95	289.95	5.63	0.021	1.27	CS	867	867.0	0.24	0.623	1.14	CS	2.46	2.462	0.14	0.706	1.08
TPP	1532.53	1532.53	29.77	0.000	1.37	TPP	98618	98618.3	27.86	0.000	1.47	TPP	429.21	429.214	25.12	0.000	1.49
pH	461.41	461.41	8.96	0.004	1.09	pH	304	303.8	0.09	0.771	1.04	pH	266.26	266.264	15.58	0.000	1.08
Quadratic	3030.73	1010.24	19.63	0.000	1.11	Quadratic	42473	14157.7	4.00	0.012	1.04	Quadratic	143.48	47.826	2.80	0.049	1.04
CS*CS	1272.96	1272.96	24.73	0.000	1.07	CS*CS	13	12.6	0.00	0.953	1.05	CS*CS	83.93	83.932	4.91	0.031	1.05
TPP*TPP	917.02	917.02	17.82	0.000	1.22	TPP*TPP	663	663.4	0.19	0.667	1.34	TPP*TPP	50.59	50.590	2.96	0.091	1.50
pH*pH	412.94	412.94	8.02	0.007	1.14	pH*pH	40169	40168.9	11.35	0.001	1.09	pH*pH	6.28	6.281	0.37	0.547	1.33
2-way interaction	629.37	209.79	4.08	0.011	1.37	2-way interaction	126510	42170.0	11.91	0.000	1.51	2-way interaction	307.57	102.524	6.00	0.001	1.38
CS*TPP	407.42	407.42	7.92	0.007	–	CS*TPP	1753	1753.5	0.50	0.485	–	CS*TPP	108.29	108.287	6.34	0.015	–
CS*pH	47.46	47.46	0.92	0.341	–	CS*pH	28239	28239.3	7.98	0.007	–	CS*pH	54.36	54.357	3.18	0.080	–
TPP*pH	78.42	78.42	1.52	0.223	–	TPP*pH	88485	88485.1	25.00	0.000	–	TPP*pH	55.69	55.688	3.26	0.077	–

RESULTS AND DISCUSSION

Response surface regression analysis using full quadratic

The integrative analysis relied on the three variables, chitosan, TPP, and pH, referred to as A, B, and C, respectively. The results represent 80 samples of nanocomposites covering the full factorial combination. These results were statistically analyzed using: i) Pareto chart, ii) contour plot, iii) surface plot, iv) interaction plot, v) main effects plot, vi) Normal probability plot, vii) versus order, viii) versus fits and ix) half normal plot. All the factors displayed are separately modeled using 1) a linear model, 2) a square model, and 3) a 2-way interaction model. Statistical analysis was conducted on all variables to understand better the nanoparticle size, loading efficiency, and zeta potential. Variables adopted for experiments and results underwent statistical analysis and included the effect degrees of chitosan, TPP, and pH with their interaction effects. A response surface regression model was used. The results are presented in Table 2. Reliability is considered to be linear and quadratic, while the 2-way interaction on the efficiency of the parameters is significant when the T-value and P-value are less than 0.05.

The analyses using the linear, square, and 2-way interaction for CS, TPP, pH, CS*CS, TPP*TPP, pH*pH, and CS*TPP showed statistical significance for these combinations. Other variables, such as CS*pH and TPP*pH, were not statistically significant. The results of the statistical analysis (ANOVA) on loading efficiency are shown in Table 3.

The variance inflation factors (VIF) describe the multicollinearity. The VIFs show an increase in the variance of an estimated regression coefficient when the predictors correlate with each other. If all the VIFs are 1, there is no multicollinearity, but if some VIFs are greater than 1, the predictors are correlated. When a VIF is > 5, the regression coefficient for that term cannot be estimated with sufficient accuracy. The results for LE (Table 3) show that the model has a low coefficient of regression variance, which corresponds with low multicollinearity.

We used a statistical model called full factorial design, a multi-linear regression design, to select the best form for the particle size. The three variables, chitosan, TPP, and pH, were used to determine the best process at multiple levels for each variable. These factors produced the best results. Eighty batches of nanoparticles were produced, and the Minitab-18 statistical software and several application program plots were applied to identify the best process. Table 3 also presents data expressing the role and impact of each of these variables on the size of the final produced nanoparticles and the results of ANOVA analysis for all variables, determining which of the variables significantly affect the size of the particles and which have no significant impact on their size.

TPP, TPP*pH, and CS*pH had a substantial, direct, and statistically significant effect on the size of the nanoparticles prepared, as demonstrated by a p-value less than 0.05 and a higher value of F. However, other variables, such as pH, CS, CS*CS, TPP*TPP, and CS*TPP, had no impact on nanoparticle size. No statistical significance was detected for these variables.

Analysis of variance for the zeta potential is shown in Table 3. P-values less than 0.05 demonstrate significance.

Linear, square, and 2-way interaction analysis models for TPP, pH, CS*CS, TPP*TPP, and pH*pH showed that these variables significantly affect zeta potential. CS, CS*pH and TPP*TPP, pH*pH, and TPP*pH variables had no statistically significant impact. Table 3 contains the variance inflation factor (VIF) values that describe the multicollinearity. If all values of VIFs are 1, then there is no multicollinearity. When the VIF values are greater than 1, then the predictors are correlated. When the VIF values are above 5, the regression coefficient is not estimated appropriately for that term. Using multiple factors in regression leads to the model being of low variance on the regression coefficient and thus considered to have low multicollinearity.

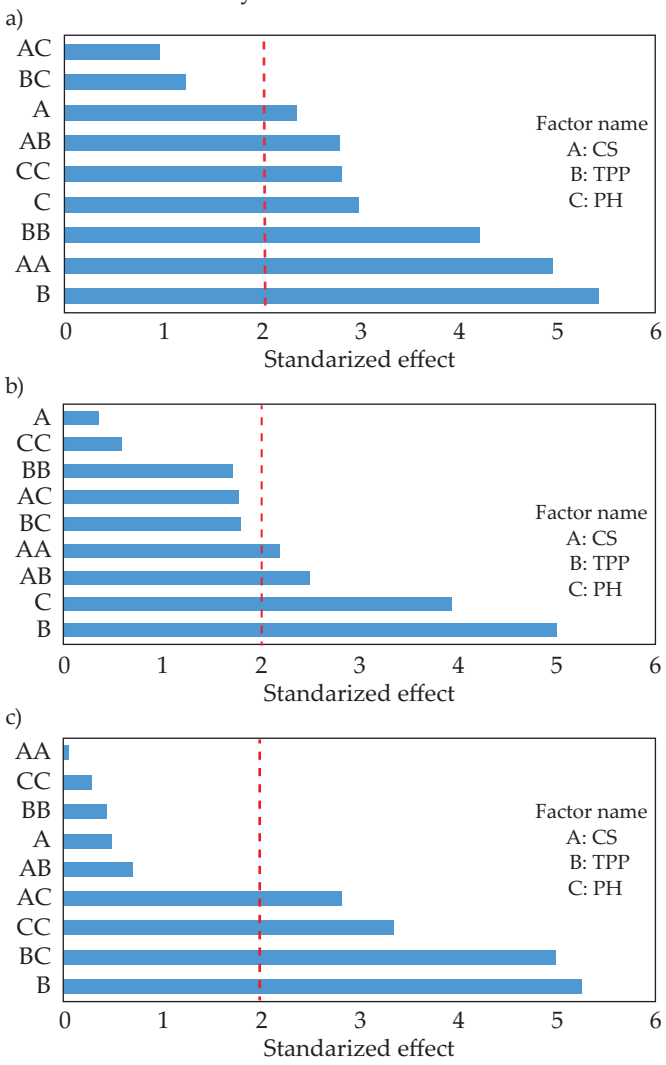

Fig. 1. Pareto charts impact: a) LE, b) zeta potential, c) particle size

Pareto charts of the effect for %LE, zeta potential, and particle size

Pareto charts are used to identify the most statistically significant effect among multiple effects, depending on a curve graph and the arrangement of the effects from the largest to the smallest.

Figure 1a shows the effect of multiple variables on the loading efficiency. The Pareto chart shows that the bars for TPP, CS*CS, and TPP*TPP interact with other variables, such as pH, pH*pH, CS*TPP, and CS, passing through the reference line at the value of 2.007. This value indicates that these factors carry a statistically significant effect on the loading efficiency at a P-level of 0.05. Also, this chart clearly shows that TPP, CS*CS, and PP*TPP had the highest significant effect on the loading efficiency compared to other variables. The loading efficiency was not statistically dependent (nonsignificant) on TPP*pH and CS*pH.

Figure 1b shows the results for the zeta potential. The Pareto chart shows that the TPP, pH, CS*TPP, and CS*CS factors cross the reference line at 2.008, indicating a strong and statistically significant influence on the zeta potential values at the 0.05 level. The plot demonstrates that TPP and pH have a more significant influence on the zeta potential than CS*TPP or CS*CS, while TPP*pH,

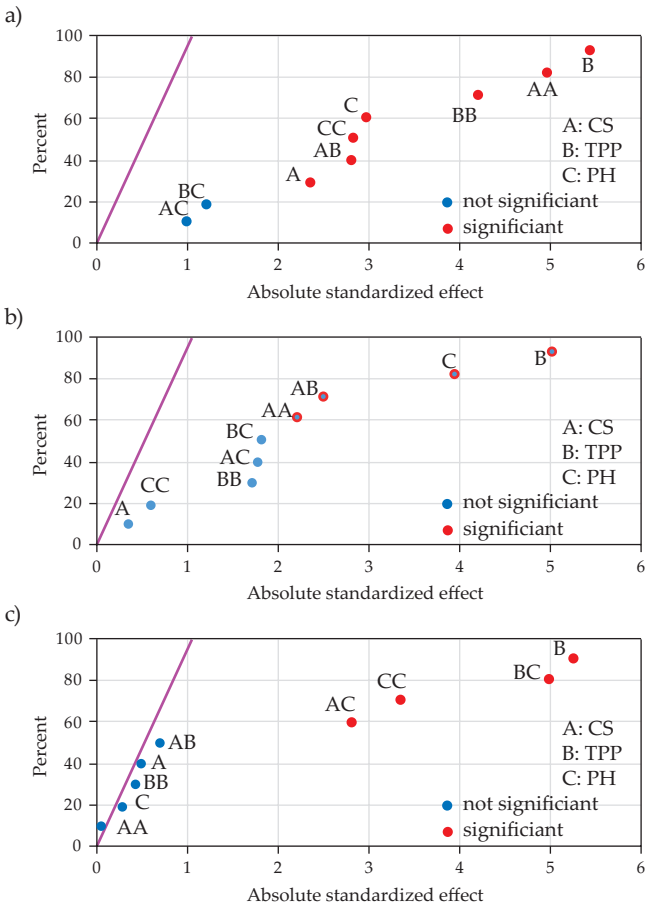

Fig. 2. Half normal plots: a) LE, b) zeta potential, c) particle size

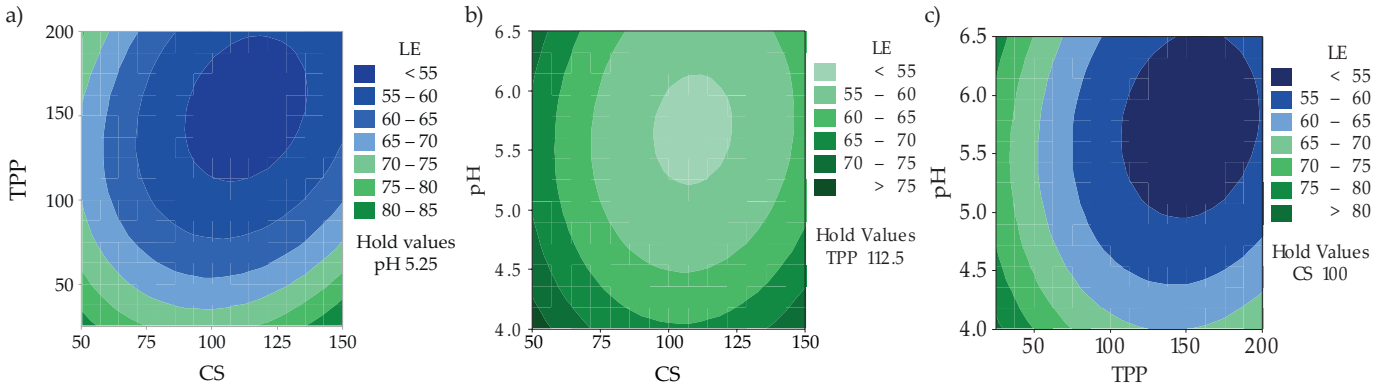

Fig. 3. Contour plots for LE against: a) TPP and CS, b) pH and CS, c) pH and TPP

CS*pH, TPP*TPP, pH*pH, and CS are not significant and have no influence.

Figure 1c shows particle size, in which the bars for TPP, TPP*pH, pH*pH, and CS*pH passes the reference line at the value of 2.004. This value means that these factors have an important and statistically significant effect on the particle size at the 0.05 level. Using the Pareto chart, we find the TPP and TPP*pH factors to have more impact on the particle size than pH*pH, CS*pH, or other variables. CS*TPP, CS, TPP*TPP, pH, and CS*CS factors are not significant and do not influence particle size.

Half normal plot effect for %LE, zeta potential, and particle size

The half-normal probability plot is used to identify and determine the magnitude and importance of any effects. The half-normal probability plot indicates that any effect further than zero is statistically significant. In these plots, the shape and color of the points are different between statistically significant and nonsignificant effects.

Parameters are labeled significant when the P-value is less than 0.05. Figure 2 demonstrates that the TPP and chitosan significantly affect LE, zeta potential, and particle size. TPP has a greater effect than chitosan in that aspect. pH significantly affected the response of zeta potential.

Contour and surface plots impact for LE, zeta potential, and particle size

The purpose of using the Contour Plot in this study is to identify the potential relationship between the three variables, Chitosan, TPP, and pH.

A contour Plot can display a two-dimensional relationship between the X and Y factors (*i.e.*, predictors) plotted on the X and Y graph. The response values are specified on the contours. The surface plot takes from a topographical map wherein x-, y-, and z-values are designed and plotted in reference to longitude, elevation, and latitude. Three dimensional (3D) surface plot is a graph that can be used to identify the potential relationship between three variables. Predictor variables are presented on the x and y scales, and here the response variable (z) appears as a smooth surface (3D diagram). The loading efficiency response is shown in Figure 3.

Figure 3c shows two regions of the highest loading efficiency (more than 80%) when pH is 6.0 to 6.5 or less than 4.3 and the amount of TPP is less than 50 mg. This data reinforces the information mentioned previously in Table 3, showing that TPP and pH were statistically significantly affecting the loading efficiency.

On the other hand, Figure 3b presents the Contour plot response analysis for the pH and chitosan relationship for the loading efficiency parameter. When the chitosan is

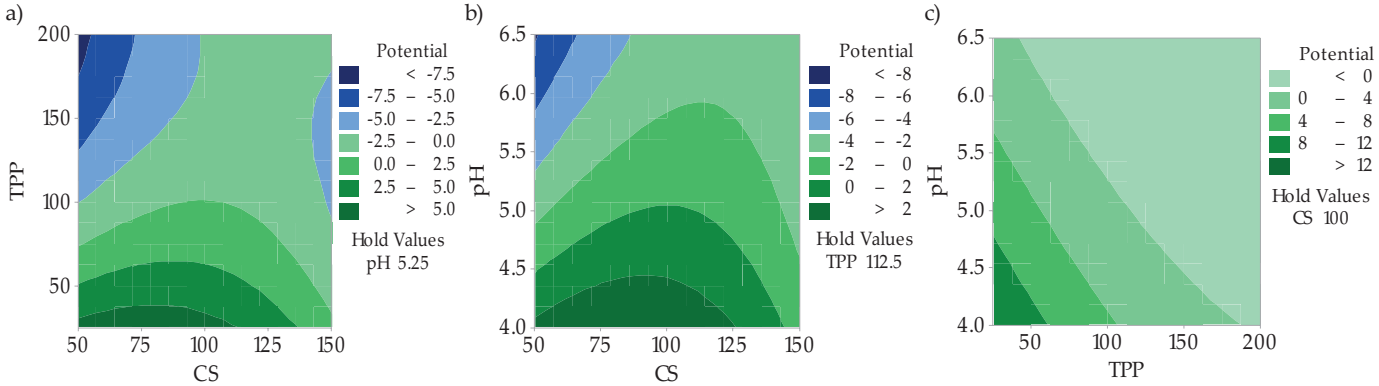

Fig. 4. Contour plots for zeta potential against: a) TPP and CS, b) pH and CS, c) pH and TPP

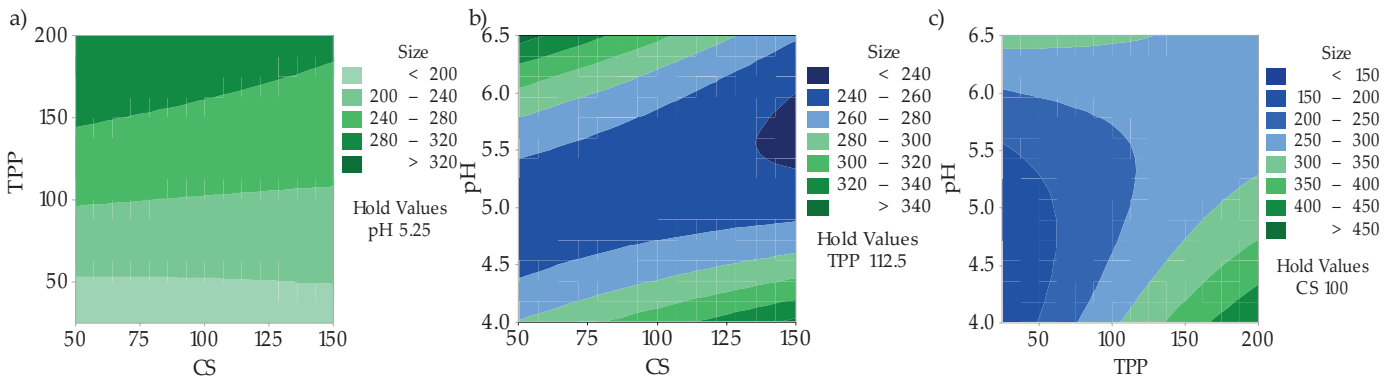

Fig. 5. Contour plots for particle size against: a) TPP and CS, b) pH and CS, c) pH and TPP

used in a small amount (about 50 mg) with a pH between 6.0 and 6.5 or less than 4.3, the loading efficiency is less than 70%. When the TPP is used at 50 mg or less and chitosan at less than 50 mg, the loading efficiency exceeds 80%. Figure 3A shows that when the CS, TPP, and pH concentrations increase, the loading efficiency decreases.

The surface plots can give a three-dimensional curvature that shows how different factors affect the process of change in the loading efficiency. This information is useful when combining the output values and various variables. The variables are displayed on the X and Y axes in these graphs, while the outputs are displayed on the Z axis. A gradient towards a darker surface implies an incremental change in response. Thus, high loading efficiency can be achieved by using approximately 50 mg of chitosan, pH around 6.0, and less than 50 mg of TPP.

Figure 4a shows that the highest zeta potential region is at pH less than 5.0, the amount of TPP is ≤ 60 mg, and the % of zeta potential is between 8–12 mV. This supports the information previously mentioned in Table 3; that is, TPP and pH explicitly affect the zeta potential value. Additionally, the Contour plots in Figure 4b present the effect of pH and the amount of chitosan on the value of zeta potential. When the amount of chitosan used is between 50 mg and 125 mg, and the pH is less than 4.5, the zeta potential increases above 2 mV. However, this value is below an effective level. Again, Table 3 shows that CS does not significantly affect zeta potential. Figure 4c) demonstrates that when TPP is less than 50 mg, and CS is between 50 and 125 mg, zeta potential is more than 5 mV which is still low. From surface plots, the highest zeta potential can be achieved using a pH of less than 5.0 and a TPP of ≤ 50 mg.

It is apparent from Figure 5c that the size of the particles is still less than 150 nm when the amount of TPP is less than 50 mg and the pH is less than 5.5. This supports the previously mentioned information in Table 3 that TPP significantly affects particle size. Furthermore, Figure 5b) demonstrates the response contour plots to the analysis of the effect of pH and amount of chitosan on the particle size. When chitosan is used in an amount of more than 125 mg, and pH is more than 5.0, the particle size reduces below 200 nm. Figure 5a shows that when TPP ≥ 150 mg, the particle size is smaller than 200 nm and has no effect on chitosan, as mentioned in Table 4. Surface plots from Figure 5c show that the size of particles is less than 50 nm when TPP is less than 50 mg and pH is less than 5.5.

Main effect plots for loading efficiency, zeta potential and particle size

A main effects plot identifies the significance of each variable on different levels. There are effects related to the role of different levels and concentrations of a given factor in producing different responses. The main effect plots curve represents the response mean for any variable associated with a line.

Figure 6a shows the main effect plot of LE, from which we conclude that chitosan, TPP, and pH are factors that have a definite effect on the loading efficiency and that, with increasing the concentration of chitosan, the loading efficiency begins to decrease until the amount of chitosan reaches 100 mg. Next, we found that increasing the amount of chitosan above 120 mg increases the value of LE. However, when the concentration of TPP increases, the LE begins to decrease until the concentration of TPP reaches 150 mg. When TPP concentration increases above 150 mg, the loading efficiency also increases. Finally, by increasing the pH, the LE begins to decrease until the pH is about 5.75. However, when pH increases above 6.0, the LE increases as well.

Figure 6b shows the main effects plot of zeta potential, which indicates that chitosan, TPP, and pH are factors that have a definite impact on the zeta potential. By elevating the chitosan concentration, the zeta potential tends to increase slightly until the amount of chitosan reaches 100 mg. The zeta potential decreases when the chitosan amount increases to more than 120 mg. When increasing the TPP concentration, the zeta potential tends to decrease until the amount of TPP reaches 200 mg. Also, by increasing pH, zeta potential tended to decrease to -2.5 mV.

Figure 6c offers the results of the main effects plot of particle size, which displays that chitosan is a factor with minimal effect on particle size, but when the TPP concentration increases, the particle size also begins to increase. When pH increases to 5.5 then the particle size tends to increase.

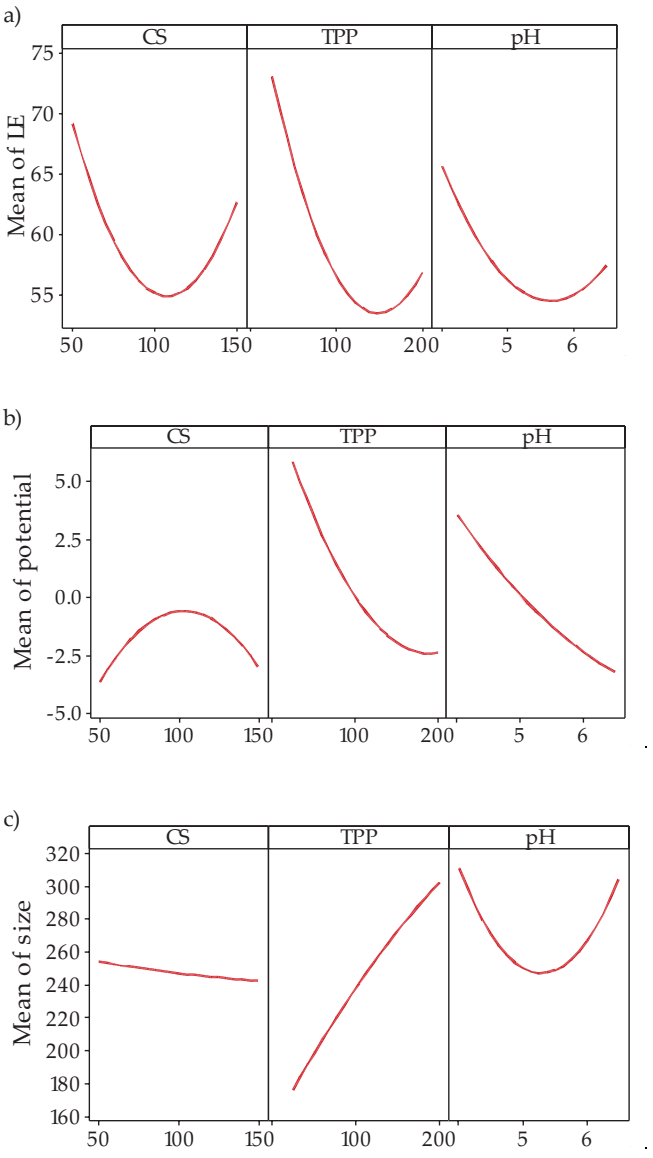

Fig. 6. Main effect plots: a) LE, b) zeta potential, c) particle size

Optimization of the loading efficiency, zeta potential, and particle size models

Optimization can be defined as selecting the best element (concerning some criteria) from some set of available alternatives. The advantage was considered for minimizing cost while maximizing profit and efficiency [23]. The optimized formula can be collected at the highest loading efficiency, smallest particle size, and optimum zeta potential. Therefore, the optimized formula should have the following parameters 39.4% LE, 322 nm particle size, and -1.33 mV zeta potential (Figure 7).

Validation of the loading efficiency, zeta potential, and particle size models

Validation ensures that a procedure carried out in the formation of a drug maintains the desired level of compliance at all stages [24]. Validation contains predicted

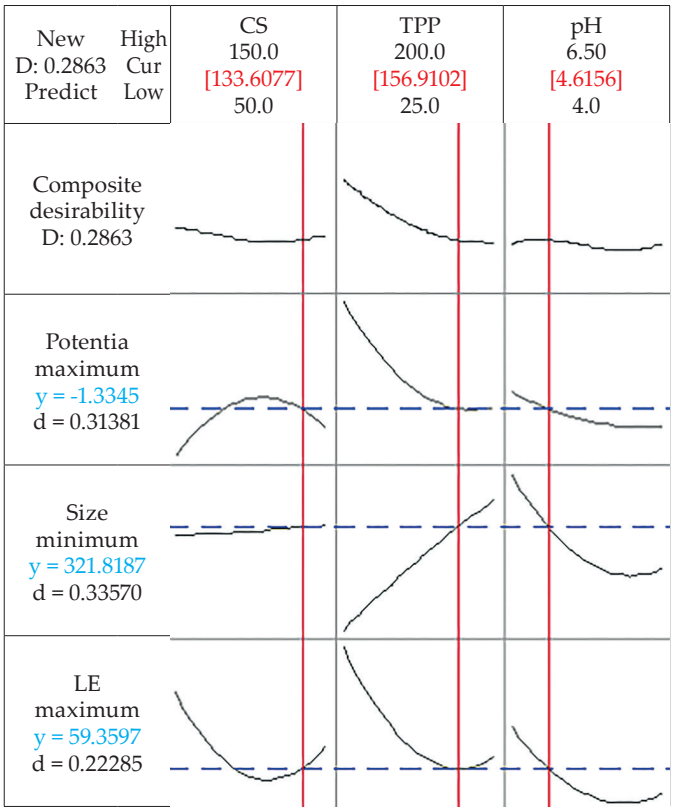

Fig. 7. Optimized concentration for response factors of LE, zeta potential and particle size

and experimental values. The model is valid when the two values are close to each other (within the allowed deviation value).

A bias formula was performed underneath optimized factors to compare the observed values with the predicted ones. Calculation of Bias was done according equation 3.

$$\%\text{Bias} = \frac{\text{Observed value} - \text{Predicted value}}{\text{Predicted value}} \cdot 100 \quad (3)$$

As demonstrated in Table 4, the amount of bias is 9.8%, -18.4%, and 20.1% for the first formula (CS=50 mg, TPP= 25 mg, and pH 4.3), respectively. The bias is -12.1%, 17%, and -17.2% for the second formula (CS=109 mg, TPP=104 mg, and pH=5.3), respectively. While the third formula had the following bias values 12.5%, -8.1%, and 8.3% for (CS=134 mg, TPP=157 mg, and pH=4.6), respectively. These are the results and data through which we conclude the validity and effectiveness of the generated models with statistically non-significant differences in addition to a good correlation between the experimental and the predicted values.

Characterization of THP-polymer nanocomposites

X-ray diffraction (XRD)

The structures of pure THP, CSNPs, and THP-CSNPs nanocomposites were characterized by the powder X-ray

T a b l e 4. Comparative results between observed and predicted response values of variables of optimized formulation

concentrations	Experimental response	Predicted values	Experimental values	Bias (%)
CS (50 mg) TPP (25 mg) pH (4.3)	LE (%)	88.8	80.1	9.8
	Particles size (nm)	342	405	-18.4
	Zeta potential (mV)	13.9	11.1	20.1
CS (109 mg) TPP (104 mg) pH (5.3)	LE (%)	55.6	62.3	-12.1
	Particles size (nm)	241	200	17.0
	Zeta potential (mV)	-0.5	-15.0	17.2
CS (134 mg) TPP (157 mg) pH (4.6)	LE (%)	59.4	52.0	12.5
	Particles size (nm)	321	347	-8.1
	Zeta potential (mV)	1.3	11.0	8.3

diffraction (XRD) technique. As presented in Figure 8, curve A is the XRD pattern of pure THP. Various sharp peaks emerged, indicating that this THP sample shows good crystallization performance. Moreover, there are diffraction peaks located at 7.28°, 12.76°, 14.54°, 22.28°, and 25.66° [25, 26]. The corresponding diffractogram of CSNPs in Figure 8b) display two amorphous peaks at 2θ of 19.1 and 24.9 with a characteristic broad hump for the second peak [27]. In addition, the THP-CSNPs nanocomposites in Figure 8C do not represent any diffraction peak for THP.

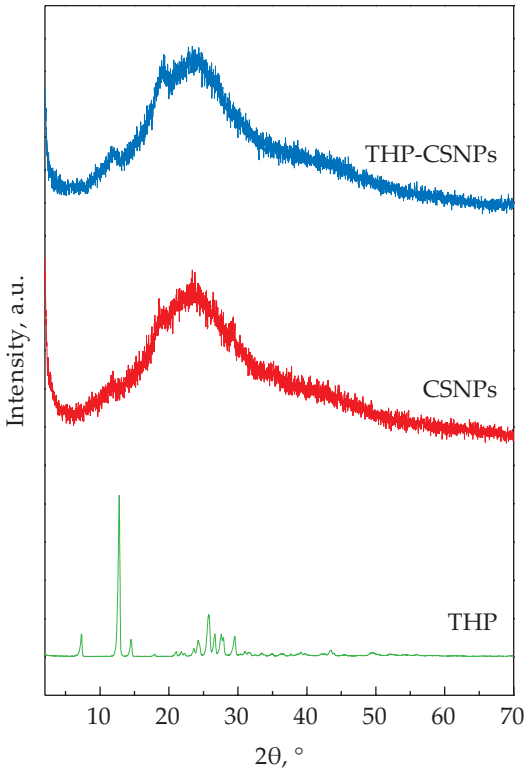

Fig. 8. Powder X-ray diffraction patterns of: THP, CSNPs, and THP-CSNPs nanocomposites

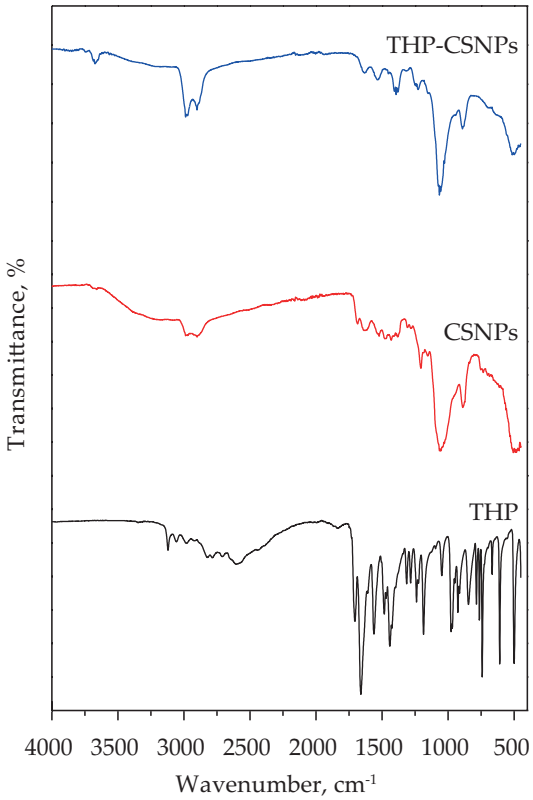

Fig. 9. FTIR spectra of: THP, CSNPs, and THP-CSNPs nanocomposites

Fourier transform infrared (FTIR)

The FTIR spectra of free THP, CSNPs, and THP-CSNPs nanocomposites are presented in Figure 9. The FTIR spectrum of THP (Figure 9a) shows an absorption band at 3120 cm^{-1}, which refers to stretching (N-H) [28]. Characteristic stretching vibrations of the carbonyl (C=O) groups of THP are present at 1706 cm^{-1} and 1659 cm^{-1}. The amine stretching signal of the THP is observed at 1562 cm^{-1} [25]. The FTIR absorption band at 1486 cm^{-1} refers to the stretching of C=C, whereas the absorption band at 1670 cm^{-1} refers to the C=N of the purine ring [29].

The unmodified chitosan shows a band at 3457 cm^{-1} corresponding to the NH_2 and OH group stretching vibrations. The broad band between 1657 cm^{-1} and 1598 cm^{-1} corresponds to the $CO\text{-}NH_2$ group and the NH_2 group bending vibration [30].

The FTIR spectra of CSNPs are presented in Figure 9b. The peak at 3447 cm^{-1} is sharp, indicating the presence of hydrogen bonding. Peaks at 1600 cm^{-1} and 1509 cm^{-1} result from the interaction between NH_3^+ groups of chitosan and phosphate groups of TPP [31]. The other significant band for CSNPs is observed at 1398 cm^{-1} owing to $-CH_2$ wagging. Furthermore, the peak at 1040 cm^{-1}, which appears in the FTIR spectra of CSNPs, shows characteristics of P=O stretching vibration from phosphate groups.

The FTIR spectrum of the THP-CSNPs nanocomposites is presented in Figure 9c). The spectrum of the nano-

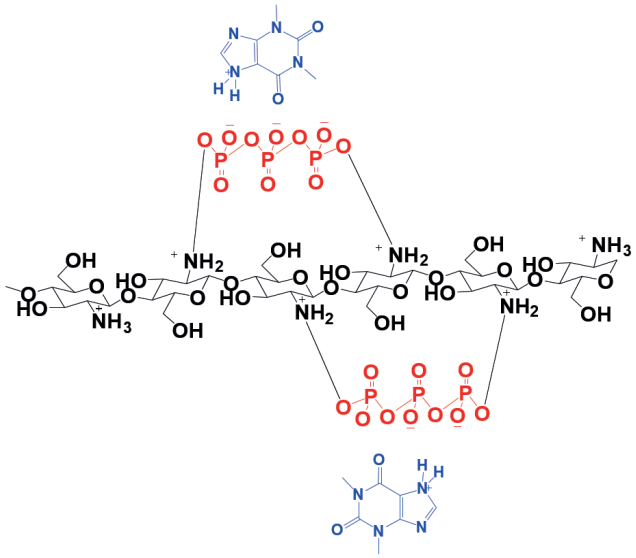

Fig. 10. Interaction of chitosan with TPP and THP in nanocomposites

composite exhibits the characteristic bands for pure THP, thus indicating that the THP interacts with the CSNP nanoparticles.

The interaction between THP and CSNPs in nanocomposites

Chitosan, with a pKa of 6.3, is polycationic when dissolved in acid and presents $-NH_3^+$ sites. In addition, sodium tripolyphosphate is dissolved in water and gives hydroxyl and phosphoric ions [32]. Therefore, the CSNPs display ionic interaction behaviors. There are three pH regimes for THP, doubly protonated at pH 2.0, singly protonated at pH 3.0, and neutral at base media above pH 8.8 [33]. The pH used in this work was between 4.0–6.5, giving the THP a positive charge. This indicates ionic interaction behavior between TPP and THP (Figure 10).

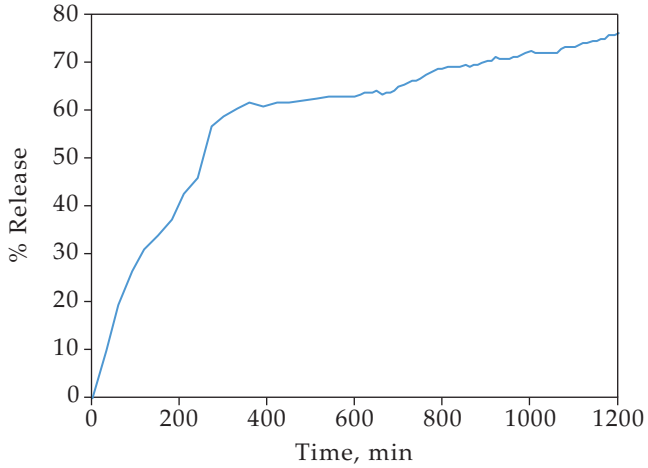

Fig. 11. In vitro release of theophylline from the prepared THP--CSNPs nanocomposites

In vitro release study of Amlop from nanocomposites

Release profile curves of theophylline from the THP-CSNPs nanocomposites are presented in Figure 11.

The release testing at pH 7.4 reports the amount released versus time. The released theophylline from nanocomposites after 10 hours reaches approximately 60%. The process of releasing theophylline from nanocomposites can be organized and explained by several mechanisms. The first method is the hydrogel swelling process by absorbing water from the release medium through the polymer and the resulting swelling and solubility that leads to the release of the drug [34]. The second explanation is the diffusion and erosion of the polymer, leading to drug release. This usually happens from the matrix containing chitosan. In diffusion, the drug permeates and penetrates through the polymer matrix to the surrounding areas. In erosion, the polymer is crushed and degraded, breaking the bonds and releasing the drug. The third explanation for the drug release process is disintegration, which depends on many factors, such as the enzymes present in the dissolution medium, the pH of the medium, and its effect on the polymer's activity. Another possibility is the interfering of samples with other polymers and taking water by these polymers, thus freeing the drug [35].

CONCLUSIONS

This study demonstrates the possibility of producing nanoparticles of theophylline with chitosan polymer by ionic gelation method with advanced and promising pharmaceutical specifications. The software Minitab 18 used in this study shows that a full factorial design can be successfully employed in developing THP-CSNPs prepared.

The prepared nanocomposite is characterized by having sustained release properties with good and stable physical properties. Particle nano-size and productive loading efficiency are acceptable, which is demonstrated by the release of the drug and its stability in the selected nanocomposites. We obtained nanoparticles with a wide nano-size range of 84–442 nm, loading efficiency between 70–80%, and stable zeta potential values. The results indicate that tripolyphosphate significantly affects LE, zeta potential, and particle size. These parameters provide great prospects for future research. We conclude that these optimized THP-CSNPs formulations will be an alternative drug delivery system for THP to enhance its bioavailability and therapeutic index.

ACKNOWLEDGMENT

The author would like to thank the Faculty of Pharmacy at Isra University for providing funding for this research under grant number 6-23-2020/2021.

REFERENCES

[1] Kennedy M.: *Drug Testing and Analysis* **2021**, *13*(*1*), 36. https://doi.org/10.1002/dta.2970

[2] Morton A., Scott C. *et al.: Journal of Allergy and Clinical Immunology* **1989**, *83*(*1*), 55. https://doi.org/10.1016/0091-6749(89)90477-6

[3] Greer F., Friars D. *et al.: Journal of Applied Physiology* **2000**, *89*(*5*), 1837. https://doi.org/10.1152/jappl.2000.89.5.1837

[4] Barnes P.J.: *American Journal of Respiratory and Critical Care Medicine* **2013**, *188*(*8*), 901. https://doi.org/10.1164/rccm.201302-0388PP

[5] Efthimiou J., Fleming J. *et al.: Thorax* **1986**, *41*(2), 122. https://dx.doi.org/10.1136/thx.41.2.122

[6] Jones D., Howell S. *et al.: Clinical Science* **1982**, *63*(2), 161. https://doi:10.1042/cs0630161

[7] DeGarmo C., Cerny F. *et al.: Journal of Allergy and Clinical Immunology* **1988**, *82*(*6*), 1041. https://doi.org/10.1016/0091-6749(88)90142-X

[8] Thompson R.T.: *American Review of Respiratory Disease* **1993**, *147*, 876. https://doi.org/10.1164/ajrccm/147.4.876

[9] Oprea A.-M., Nistor M.-T. *et al.: Carbohydrate Polymers* **2012**, *90*(*1*), 127. https://doi.org/10.1016/j.carbpol.2012.05.004

[10] Naahidi S., Jafari M. *et al.: Journal of Controlled Release*, **2013**, *166*(2), 182. https://doi.org/10.1016/j.jconrel.2012.12.013

[11] Park K.: *Journal of Controlled Release* **2014**, *190*, 3. https://doi.org/10.1016/j.jconrel.2014.03.054

[12] Weber C., Coester C. *et al.: International Journal of Pharmaceutics* **2000**, *194*(*1*), 91. https://doi.org/10.1016/S0378-5173(99)00370-1

[13] Yih T., Al-Fandi M.: *Journal of Cellular Biochemistry* **2006**, *97*(*6*), 1184. https://doi.org/10.1002/jcb.20796

[14] Herman E., Zhang, J. *et al.: Cancer Chemotherapy and Pharmacology* **1997**, *40*(*5*), 400. https://doi.org/10.1007/s002800050677

[15] De Jong W.H., Borm P.J.: *International Journal of Nanomedicine* **2008**, *3*(2), 133. https://doi.org/10.2147/IJN.S596

[16] Jeong Y.-I., Jin S.G. *et al.: Colloids and Surfaces B: Biointerfaces* **2010**, *79*(*1*), 149. https://doi.org/10.1016/j.colsurfb.2010.03.037

[17] Hadwiger L.A.: *Plant Sciences* **2013**, *208*, 42.

[18] Mohammed M.A., Syeda J.T. *et al.: Pharmaceutics* **2017**, *9*(*4*), 53. https://doi.org/10.3390/pharmaceutics9040053

[19] Zhao H., Wei Y. *et al.: Nano letters* **2015**, *15*(*12*), 7927. https://doi.org/10.1021/acs.nanolett.5b03003

[20] Feng Z.Q., Sun C.G. *et al.: Drying Technology* **2015**, *33*(*1*), 55. https://doi.org/10.1080/07373937.2014.935857

[21] El-Sherbiny I. M., Smyth H.D.C.: *Molecular Pharmaceutics* **2012**, *9*(2), 269.

[22] Pant A., Negi J.S.: *European Journal of Pharmaceutical Sciences* **2018**, *112*, 180. https://doi.org/10.1016/j.ejps.2017.11.020

[23] Bernardo F.P., Pistikopoulos E.N. *et al.: Computers and Chemical Engineering* **2001**, *25*(*1*), 27. https://doi.org/10.1016/S0098-1354(00)00630-X

[24] Whittemore R., Chase S.K. *et al.: Qualitative Health Research* **2001**, *11*(*4*), 522. https://doi.org/10.1177/104973201129119299

[25] Trivedi V., Nandi U. *et al.: Drug Delivery and Translational Research* **2018**, *8*(*6*), 1781. https://doi.org/10.1007/s13346-018-0478-8

[26] Wardhana Y.W., Tedjasaputra M.G.: *Jurnal Sains Materi Indonesia* **2018**, *12*(2), 141. https://DOI.10.17146/jsmi.2011.12.2.4605

[27] Kalaivani R., Maruthupandy M. *et al.: Frontiers in Laboratory Medicine* **2018**, *2*(*1*), 30. https://doi.org/10.1016/j.flm.2018.04.002

[28] Ismail A.H., Al-Bairmani H.K. *et al.: Nano Biomedical Enginering* **2020**, *12*(2), 139. https://DOI:10.5101/nbe.v12i2.p139-147

[29] Gacki M., Kafarska K. *et al.: Crystals* **2020**, *10*(2), 97. https://doi.org/10.3390/cryst10020097

[30] Hussein-Al-Ali S.H., Kura A. *et al.: Polymer Composites* **2018**, *39*(2), 544. https://doi.org/10.1002/pc.23967

[31] Lustriane C., Dwivany F.M. *et al.: Journal of Plant Biotechnology* **2018**, *45*(*1*), 36. https://doi.org/10.5010/JPB.2018.45.1.036

[32] Bhumkar D.R., Pokharkar V.B.: *Aaps Pharmscitech* **2006**, *7*(2), E138. https://doi.org/10.1208/pt070250

[33] Santos C.I., Ramos M.L. *et al.: The Journal of Chemical Thermodynamics* **2017**, *110*, 162. https://doi.org/10.1016/j.jct.2017.02.019

[34] Mahdavinia G.R., Mosallanezhad A. *et al.: International Journal of Biological Macromolecules* **2017**, *97*, 209. https://doi.org/10.1016/j.ijbiomac.2017.01.012

[35] Fonseca-Santos B., Satake C.Y. *et al.: International Journal of Nanomedicine* **2017**, *12*, 6883. https://doi: 10.2147/IJN.S138629

Received 17 XII 2022.